Experimental Testing of a Real Aggregator System Performing Rigorous Optimal Control of Electrical and Thermal Storage

Christopher Challen[a,*], Max Jensen[b], Spyros Skarvelis-Kazakos[a]

[a]*School of Engineering and Informatics, University of Sussex, Brighton, BN1 9QT, UK*
[b]*School of Mathematical and Physical Sciences, University of Sussex, Brighton, BN1 9QH, UK*

Abstract

This paper provides an experimentally validated optimal control approach based on a Hamilton–Jacobi–Bellman (HJB) model for optimising aggregated distributed energy resources across multiple energy carriers. The research incorporates nonlinear effects arising from storage degradation, conversion efficiency and self-discharge as well as multiple energy carrier storage. A semi-Lagrangian HJB solver was implemented on low-cost digital controllers, and integrated into a real fully functional cloud-based aggregation platform. The computational cost is kept at a minimum, enabling on-line computations on the low-cost controller, while maintaining a rigorous proof of convergence to the theoretical value function of the nonlinear, non-convex optimal control problem.

The controller links into a distributed optimal control platform that is using local as well as cloud-based information and performs all the computation and decision-making locally. The distributed controllers were tested and validated on site with an electrical and a thermal storage device. Experimental results confirm that the framework is practical, accommodates nonlinear effects and inaccurate external forecasts, has a small computational cost, is robust and can deliver significant cost benefits to the stakeholders.

Keywords: energy storage, optimal control, energy management, aggregation, multiple energy carriers, integrated energy system

1. Introduction

Multiple energy carriers, otherwise referred to as integrated energy systems or multi-vector energy systems, have been introduced as a research concept several years ago, by defining the Energy Hub unit [1, 2]. An Energy Hub is considered to be a closed system with energy inputs and outputs of multiple types, and internal conversion components. These internal components are typically used to convert energy between energy carriers, but can also include demand-side management and energy storage as a buffer between inputs and outputs [3]. The relationships between inputs and outputs are described by a coupling matrix [1]:

$$\begin{bmatrix} L_a \\ \vdots \\ L_b \end{bmatrix} = \begin{bmatrix} D_{ac} & \cdots & D_{bc} \\ \vdots & \ddots & \vdots \\ D_{ad} & \cdots & D_{bd} \end{bmatrix} \cdot \begin{bmatrix} P_c \\ \vdots \\ P_d \end{bmatrix} \tag{1}$$

The elements of the coupling matrix are representations of the conversion devices that are included in the hub.

A key benefit of incorporating energy storage in energy hub optimisation is that it can be used to offset variability caused by renewables [4], even in a residential context [5].

Yet, a comprehensive representation of the physical energy hub through a model requires replication of highly nonlinear and non-convex effects. Dealing with these effects proves to be challenging, not least because gradient-based optimization methods are often inefficient and tend to convergence to local minima, as outlined in the recent review in [6]. In that review, it is also highlighted how metaheuristic nonlinear programming as well as machine learning approaches, while computationally efficient, may lack the necessary guarantees needed for the independent operation of an energy system.

For this reason dynamic programming techniques have recently attracted great interest for the robust, realistic and efficient energy management of small and mid-sized energy systems. In this article we propose the use of energy hubs linked as distributed dynamic programming platform through a cloud-based information system. When considering time and charge levels as continuous variables the dynamic programming principle leads to an Hamilton–Jacobi–Bellman partial differential equation.

A central component of our work is the full experimental validation of the optimal control model in a testing laboratory, assessing the ramifications arising from modelling assumptions as well as forecasting inaccuracies.

*Corresponding author
Email addresses: C.Challen@sussex.ac.uk (Christopher Challen), M.Jensen@sussex.ac.uk (Max Jensen), S.Skarvelis-Kazakos@sussex.ac.uk (Spyros Skarvelis-Kazakos)

We highlight other recent developments for the optimal control of small and mid-sized energy systems with dynamic programming. In [7] battery management was compared with and without weather prediction, using a discrete control model for a single energy carrier. The resulting algorithm was predicted to be computationally efficient for implementation on battery controllers. A linear programming optimal control formulation was proposed in [8], taking real-time predictions into account, using data from the Pecan Street Project. A piecewise quadratic control model with a single energy carrier was solved in [9], and the results validated at the Biling substation, China. Here charge and discharge constraints were added to prolong the storage life expectancy. Finally, [10] uses dynamic programming to assess the optimal investment into photovoltaic generation and storage in domestic settings.

We note that none of these approaches has considered whether the proposed algorithms will approximate the theoretically optimal control increasingly well as the time step and storage charge levels are refined, noting that time and charge levels are physically continuous quantities. Yet, the approximation of entirely incorrect spurious solutions is a well-documented problem of dynamic programming, e.g. see [11, Section 1.4] and [12, Section 1.5], which is addressed in this work.

In [13] the semi-Lagrangian HJB approach was recently compared with direct NLP techniques in a setting with a single electrical storage device and a diesel generator. Even though the nonlinear structure of the optimal control problem in [13] differs from ours, the work provides evidence that this approach is well-suited to energy storage problems, as it is linearisation-free, computationally efficient and provides globally optimal solutions.

We now turn to optimal control of multi-carrier residential energy systems. Setups with multi-carrier energy sources and demands are, for example, analysed in [14], [15]; we refer also to the references therein. Generally, the application of multiple energy carrier microgrids is widespread, ranging from residential micro-hubs to commercial and agricultural macro-hubs, as reviewed in [16]. On district level, multi-carrier storage has been modelled in [17]. When it comes to a local residential focus, this reduces the problem size on the one hand, but on the other hand it also increases uncertainty, due to the lack of multi-customer load diversity [18].

Forecasting methodologies in connection with optimal control models and strategies to deal with uncertainty in forecasting have been compared in [19]. From the assessment in [19], we find that the deterministic look-ahead strategies are competitive for a range of storage applications, while computationally efficient. In order to enable the predictive computation of optimal controls on storage control units, we embed one such strategy in this work, where forecasts are generated by a cloud-based industrial provider [20]. Alternative forecasting techniques are outlined in [21], regarding photovoltaic power generation, and in [22], regarding energy consumption.

Optimisation of energy systems typically is either organised centrally, hierarchically or in distributed form [23]. Distributed control in the energy system context has been a developing research field, and local controllers are often referred to as intelligent, since they can perform advanced functions beyond simple automation [24]. Agent-based control is one form of intelligent control that has long been under development for use by the energy industry [25]. The extension of agent-based control to multiple energy carrier systems was previously proposed by the authors in [26], which combines the benefits of distributed control with the integration of energy systems. Different layers of aggregation and control localisation can be considered, depending on the application, but it is logical to assume that the energy hub will be one of the layers. A similar approach was proposed in [27], where electric vehicles are considered to have a similar functionality as energy storage. Furthermore, distributed control improves the scalability of the system, especially compared to central control, and more easily accommodates privacy and data protection concerns. Due to the above benefits of local control, the framework proposed in this paper is based upon the concept of local optimisation controllers, and in some respects an extension of the work published by the authors in [26].

The practical implementation of such control methodologies requires interoperability with current industrial practices. One example is the use of existing smart home equipment, such as Home Automation Systems (HAS) or smart meters [28]. Typically, an aggregator server is required centrally, to co-ordinate the operation of multiple residential devices, as well as interface with the market and other entities [28]. Experimental implementations often rely on SCADA systems and communication protocols such as Modbus and OPC UA, which can sometimes be found in real microgrids, but rarely in residential premises [29]. Real smart grid communications often involve more agile platforms, such as ZigBee and Home Area Networks (HAN), which are used in commercial smart meters [30]. At the local level, such commercial platforms can provide sufficient capability, and this capability is augmented by cloud-based services, which are becoming more popular for smart grid applications [31]. Such implementation architectures have also been applied to energy storage controllers [32]. The key challenge in such distributed and local implementations is for the system to be able to perform local optimisation rigorously and efficiently, on small-scale platforms that are computationally constrained.

Following the above literature gaps, the key contributions of this paper can be summarised as follows:

- The experimental validation of a novel optimally controlled energy hub methodology, which confirmed significant cost savings compared to the conventional balance mode.
- Incorporation of the nonlinear effects of storage degradation, conversion efficiency as well as self-discharge

into a model of energy hubs with multi-carrier energy storage devices.

- A computational control framework that approximates the continuous-time optimal control problem rigorously, despite non-convex nonlinearities. The optimal control algorithm returns controls for the whole state space and time horizon, ensuring a controlled, operational aggregator system even when the environment deviates from the cloud-supplied forecasts.
- The enabling advantage of the proposed method is the combination of computational efficiency, allowing adaptive rolling horizon updates on a Raspberry Pi controller under operational conditions, with a robust, non-heuristic optimal control formulation.
- All aspects of the methodology are implemented experimentally and validated with a real-life operational aggregation platform (GridShare). In order to align this research with current industrial agent practices, the implementation was designed in line with the recently published developments IEEE 2660.1-2020 Recommended Practice [33].

The remainder of the paper consists of the model description (Section 2), a case study (Section 3) and simulations and experimental validation (Sections 4 and 5). Conclusions are drawn in Section 7. Subsection 2.1 proves convergence of the optimization method.

2. Model

We present a mathematical model to perform multiple energy carrier optimisation within an energy hub containing energy storage devices. The aim is to supply the forecasted loads at the lowest possible financial cost. The coupling equation to quantify these interactions is given by the identity:

$$L = \begin{bmatrix} D_s & D_f & D_i \end{bmatrix} \cdot \begin{bmatrix} P_s \\ P_f \\ P_i \end{bmatrix}. \tag{2}$$

Here L is a vector representing the loads, P_s the powers at the energy storage devices, P_f the powers at the flexible power sources and P_i the powers at the inflexible power sources, respectively. Finally, $D = [D_s, D_f, D_i]$ is the coupling matrix, consisting of the sub-matrices D_s, D_f and D_i. An inflexible power source represents a source where the power output cannot be controlled, such as solar photovoltaic where the power output is subject to the local weather conditions. A flexible power source by contrast represents a source where the power can be controlled by the hub, such as power drawn from the electrical grid.

The controls $v = (v_1, \ldots, v_m)^T$ of the system determine the powers at the storage devices and flexible power sources through a matrix A:

$$\begin{bmatrix} P_s \\ P_f \end{bmatrix} = A \cdot v. \tag{3}$$

We ensure that loads $L \in \mathbb{R}^n$ can be supplied with the requirement that A is such that for any L there is a v solving $L = [D_s, D_f] \cdot A \cdot v + D_i P_i$. Mathematically, this means that the rank of $[D_s, D_f] \cdot A$ is equal to the number n of loads. In interesting scenarios v is not unique and it is the aim of this paper to choose the v which minimises the operational costs.

Energy stored in the jth storage unit is constrained by the minimum and maximum State Of Charge level (SOC) of the storage unit:

$$C_j^{\min} \leq C_j \leq C_j^{\max}. \tag{4}$$

The charges C are related to the powers P_s through the ordinary differential equation

$$\mathrm{d}_t C = R(P_s, C). \tag{5}$$

For an ideal storage device $R(P_s, C) = P_s$, but generally R is subject to charging and discharging inefficiencies as well as energy dissipation and may be nonlinear.

Each power flow $P_j \in \mathbb{R}$ in the P_s, P_f and P_i vectors may be constrained from below by a $P_j^{\min}$, i.e. $P_j^{\min} \leq P_j$, and from above by a $P_j^{\max}$, i.e. $P_j \leq P_j^{\max}$. In case of a storage device $P_j^{\min}$ is typically negative and called the peak charging rate, and $P_j^{\max}$ is typically positive and called the peak discharging rate. The constraints (4) can now be realised through additionally restricting P_j at minimum and maximum SOCs; we confine the admissible P_j at $C_j^{\min}$ to exclude further discharging and at $C_j^{\max}$ to exclude further charging:

$$\begin{aligned} R(P_s, C_j^{\min}) &\geq 0, \\ R(P_s, C_j^{\max}) &\leq 0. \end{aligned} \tag{6}$$

The cost functional consists of three terms: Firstly, the forecasted cost of energy to satisfy demand is a time-dependent running cost (7). This cost is derived from the coupling equation as the product of the energy consumed from or sold to the power sources P_f and P_i with their associated financial costs F_f and F_i:

$$\ell_{EC} = P_f F_f + P_i F_i. \tag{7}$$

Secondly, the cost for storage degradation, also a running cost, which is a function of P_s:

$$\ell_{SD} = \ell_{SD}(P_s). \tag{8}$$

Often $\ell_{SD}(P_s)$ is represented through a quadratic penalty, i.e. $\ell_{SD}(P_s) = P_s^2 \cdot F_{SD}$, where F_{SD} is the storage degradation coefficient and has the unit $£/(W^2 h)$.

Finally, the monetary value of energy in the storage devices at the end time T of the forecasted period contributes a (negative) terminal cost, where F is the value

associated with the energy type released by the storage device:

$$\psi = -C(T) \cdot F(T). \tag{9}$$

Let $\ell = \ell_{EC} + \ell_{SD}$. Then the forecasted cost is

$$\mathcal{J} = \int_t^T \ell(\tau)\,\mathrm{d}\tau + \psi, \tag{10}$$

which depends on the current time t and current SOC C as well as the scheduled control $v(\tau)$, which is a function of time for $\tau \in [t, T]$.

The value function represents the forecasted cost at time t with SOC C under optimal control:

$$u(t, C) = \min_v \mathcal{J}(t, C, v). \tag{11}$$

Owing to the dynamic programming principle, cf. [34], we find for small time steps Δt that

$$u(t, C) \approx \min_v \left[\Delta t \cdot \ell(t) + u(t + \Delta t, C + \Delta C)\right], \tag{12}$$

where $C + \Delta C$ is the updated SOC at $t + \Delta t$ via (5):

$$\Delta C = C(t + \Delta t) - C(t) = \int_t^{t+\Delta t} R(P_s(\tau), C(\tau))\,\mathrm{d}\tau. \tag{13}$$

The minimisers on the right-hand side of (12) provide the optimal controls of the model [34].

The right-hand side of (13) provides a discretisation of the optimal control problem in time. Also the dependence on the state variable needs to be fully discretised in order to arrive at a system with a finite number of degrees of freedom. For that purpose we represent u at each time step through a continuous piecewise linear finite element function. At this point we obtain then a semi-Lagrangian approximation of the value function, following the derivation of [35, Section 3].

2.1. Convergence proof of the numerical method

In this subsection we prove that the semi-Lagrangian solution approximates the true value function arbitrarily well through sufficient mesh and time step refinement, even when D depends nonlinearly on P and the states of the storage devices.

The numerical solution at the jth time step is $u_j \approx u(j\,\Delta t)$. It belongs to a piecewise linear continuous finite element space on a triangulation of the state space

$$\boldsymbol{C} := [C_1^{\min}, C_1^{\max}] \times \cdots \times [C_k^{\min}, C_k^{\max}],$$

where k is the number of storage devices. The numerical solution satisfies the scheme

$$u_j(C) = \min_v \left[\Delta t \cdot \ell(t, C, v) + u_{j+1}(C_{+\Delta t})\right], \tag{14}$$

where $C_{+\Delta t} = C + \Delta t\, R(P_s(v), C)$ is (approximately) the state of charge at the $(j+1)$st time step when applying control v at the jth step at state of charge C, discretising (13). Here $P_s(v)$ is given by (3). The control v ranges in (14) through $\mathbb{R}^m$, subject to $P_s(v) \in [P_1^{\min}, P_1^{\max}] \times \cdots \times [P_k^{\min}, P_k^{\max}]$ and $C_{+\Delta t} \in \boldsymbol{C}$, consistent with (6). Let Δx be the largest element diameter. All constants are assumed independent of Δt and Δx.

Theorem 1. *Suppose ℓ, ψ are continuous with Hölder exponent $\gamma \in (0, 1]$ and R is Lipschitz. Then there is a $c_1 > 0$ such that*

$$|u_j(C) - u(j\,\Delta t, C)| \le c_1 \left(\frac{(\Delta x)^\gamma}{(\Delta t)^{\gamma/2}} + (\Delta t)^{\gamma/2}\right)$$

at all time steps j and charge levels C if there is a constant $c_2 > 0$ with $\frac{\Delta x}{\Delta t} < c_2$.

Proof. Following [34], the exact value function u of (11) satisfies $-\partial_t u + \mathcal{H}u = 0$ with $u(T) = \psi$ as viscosity solution where $\mathcal{H}u = \sup_v[-R(t, C, v) \cdot \nabla u - \ell(t, C, v)]$.

Owing to the chain rule,

$$\hat{u}(t, C) = u(t, C)\,\exp(\lambda t)$$

solves $-\partial_t \hat{u} + \lambda \hat{u} + \mathcal{H}\hat{u} = 0$ for $\lambda > 0$ and $\hat{u}_j = u_j \exp(\lambda t)$ solves, importantly, (14) of [35] for this modified Bellman equation. Noting that (28) of [35] follows from $C_{+\Delta t} \in \boldsymbol{C}$, the a priori convergence bound [35, Theorem 3.1] applies to $\hat{u}_j$. Finally, $\|u_j - u(j\Delta t)\|_\infty = \exp(-\lambda j \Delta t)\|\hat{u}_j - \hat{u}(j\Delta t)\|_\infty$. □

The set of controls in the minimisation of (14) may be discretised in the computer implementation without losing convergence [36, part 2 of section 3].

This convergence proof stands in contrast to guarantees which can be given with NLP solvers, which directly minimize the cost subject to (discretisations of) the constraints (2)–(6) because NLP solvers are generally not guaranteed to find the global optimum of such nonlinear, non-convex problems. In this context the brute force approach of investigating all possible paths is not advisable: even though it would surely provide the global optimum of the nonlinear, non-convex problem, the number of paths increases exponentially with the number of time steps (given a fixed discretisation of the control set and of the other parameters). In contrast the computational cost of the HJB discretisation increases on linearly in $1/\Delta t$, other parameters being fixed.

3. Case Study

The case study in this work considers a residential property equipped with an electrical energy storage device, a thermal energy storage device and an array of photovoltaic solar generation cells (PV). The energy hub diagram, cf. Fig. 1, shows the interactions between the loads, external energy sources, energy converters, and storage devices. Throughout the subsequent text the subscript E represents the electrical grid, R renewable electrical, T

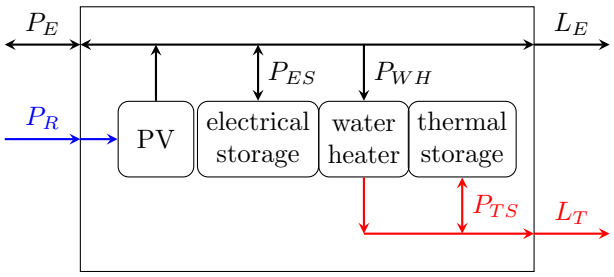

Figure 1: Energy hub with electrical (——), thermal (——) and solar (——) power flows.

thermal, WH water heater, ES electrical storage and TS thermal storage.

The coupling equation, following (1),

$$\begin{bmatrix} L_E \\ L_T \end{bmatrix} = \begin{bmatrix} 1 & \eta_{PV} & \eta_{ES} & -1 & 0 \\ 0 & 0 & 0 & \eta_{WH} & \eta_{TS} \end{bmatrix} \cdot \begin{bmatrix} P_E \\ P_R \\ P_{ES} \\ P_{WH} \\ P_{TS} \end{bmatrix} \tag{15}$$

quantifies these interactions. The letter η denotes efficiencies, in combination with the respective subscript. The efficiency coefficients η_{ES} and η_{TS} depend nonlinearly on P. Here η_{ES} is an efficiency factor that is linked to the charging and discharging efficiency of the storage device, and during charging ($P_{ES} > 0$) it is equal to the inverse of the charging efficiency:

$$\eta_{ES}(P_{ES}) = \begin{cases} \eta_{ES}^{D} & : P_{ES} \leq 0, \\ 1/\eta_{ES}^{C} & : P_{ES} > 0. \end{cases} \tag{16}$$

The relationships between η_{TS}^{C}, η_{TS}^{D} and η_{TS} are analogous.

The power flow P_R is inflexible. Also L_E and L_T are determined externally and are not controllable. The power flow P_{WH} is uni-directional, i.e. subject to a one-sided constraint. There are two controllable units within the system, namely the electrical storage and thermal storage units. These controls are referred to as v_{ES} and v_{TS}, respectively, with $v_{ES} = P_{ES}$ and $v_{TS} = P_{TS}$. Hence A is an identity matrix.

Equations (2)–(12) are used in combination with (15)–(16) to create the specific equations (17)–(22) for this case study. F_{SD} is selected empirically as $10^{-6}£/(W^2/h)$.

The following inputs must be provided to the optimiser:

1. **Forecasts:** Electrical and thermal loads, PV generation, and electricity price.
2. **Non-controllable constraints:** Charge limits, efficiencies, storage capacities, power constraints, and self-discharge rates.
3. **State space parameters:** Forecast duration, time step size, number of discretised dispatch factor steps, and number of discretised SOC steps.

Remark: Theorem 1 applies for the specific model (17)–(22) of the case study with the dimension of the domain $k = 2$ and the Hölder exponent $\gamma = 1$. Then, if $\frac{\Delta x}{\Delta t}$ remains constant in the course of the refinement, we find the guarantee that

$$\|u_j(C) - u(j\,\Delta t, C)\|_\infty \leq c_3(\Delta t)^{1/2} \leq c_4(\Delta x)^{1/2}$$

for some constants $c_3, c_4 > 0$.

3.1. Assumptions

Two 72 hour datasets were created using the CREST Demand Model [37] to evaluate the optimisation model during periods of summer and winter, corresponding to high and low PV energy generation, respectively. In both cases the storage units begin at 100% SOC and run initially for 48 hours to allow the system to settle into a steady state. The results from the subsequent 24 hours are used for evaluation and the corresponding forecasts are shown in Fig. 2. It was considered if energy stored in a storage unit at the end of study period should be equal to the initial value, as in [5], but was decided that this was unrealistic. The demand profiles were created for a dual occupancy terraced residential building in Brighton, UK; fitted with a 10 m^2 photovoltaic array (selected in accordance with the standard CREST configuration), a 4.8 kWh Moixa solar electrical storage battery [38], and a 3.5 kWh SunampPV thermal storage battery [39].

The electricity prices are given by the Npower 'Go Green Energy Fix' tariff in 2019, with an Economy 7 meter [40]. The seven low cost hours are from 23:00 until 06:00 daily. The value of electricity sold to the grid is 0.0379 £/kWh, in accordance with the 2019 Feed-in Tariff higher rate for 0–10 kW standard solar PV [41]. All UK tariff rates are currently fixed at single or dual rates; however, the optimiser is able to check the tariff rate at every time step, so it can be used in countries where electricity prices fluctuate throughout the day.

Forecasting platforms such as GridShare [20] operated by Moixa offer a single scenario as forecast. A crucial benefit of the dynamic programming approach is that the numerical solution of the underlying HJB equation allows us to evaluate the whole state space efficiently, ensuring the availability of controls when forecasts deviate from real consumption and prices. Furthermore, in this framework, forecasting errors can be mitigated through the use of a receding horizon control [42]. This is defined as the rerunning of the optimiser at regular intervals, or following significant discrepancies between forecasted and actual loads.

The electrical storage unit is prevented from operating below 20% SOC by the manufacturer. The thermal storage unit is only used for domestic hot water in this study, not for space heating, so this component has been removed from the CREST demand models. Table 1 summarises the unit capacities, constraints, efficiencies, and optimisation parameters.

$$u(t, C_{ES}, C_{TS}) = \min_{v_{ES}, v_{TS}} \mathcal{J}(t, C_{ES}, C_{TS}, v_{ES}, v_{TS}), \tag{17}$$

$$\ell_{EC} = \left[-L_E - P_R \cdot \eta_{PV} - v_{ES} \cdot \eta_{ES}(v_{ES}) - \min\left(\frac{L_T + v_{TS} \cdot \eta_{TS}(v_{TS})}{\eta_{WH}}, 0 \right) \right] \cdot F_E, \tag{18}$$

$$\ell_{SD} = (v_{ES}^2 + v_{TS}^2) \cdot F_{SD}, \tag{19}$$

$$\psi = [-C_{ES}(T) - C_{TS}(T)] \cdot F_E(T), \tag{20}$$

$$\mathrm{d}_t \begin{bmatrix} C_{ES} \\ C_{TS} \end{bmatrix} = \begin{bmatrix} -\eta_{ES}(v_{ES}) \cdot v_{ES} - D_{ES} \cdot C_{ES} \\ -\eta_{TS}(v_{TS}) \cdot v_{TS} - D_{TS} \cdot C_{TS} \end{bmatrix}, \tag{21}$$

$$u(t, C_{ES}, C_{TS}) \approx \min_{v_{ES}, v_{TS}} \left[\Delta t \cdot \ell(t, v_{ES}, v_{TS}) + u(t + \Delta t, C_{ES} + \Delta C_{ES}(v_{ES}, v_{TS}), C_{TS} + \Delta C_{TS}(v_{ES}, v_{TS})) \right]. \tag{22}$$

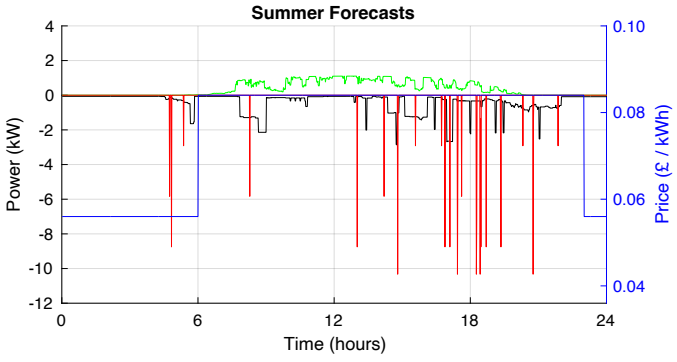

(a) Summer forecasts

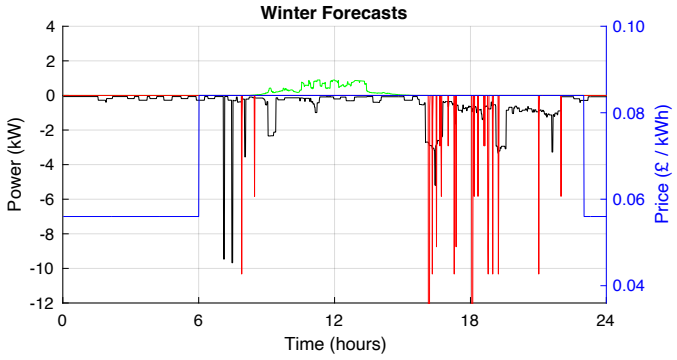

(b) Winter forecasts

Figure 2: Forecasts of PV generation (——), electrical load (——), thermal load (——) and electricity price (——)

Description	Value
Electrical storage capacity C_{ESM}	4.8 kWh
Electrical storage minimum charge C_{ESm}	0.96 kWh
Thermal storage capacity C_{TSM}	3.5 kWh
Thermal storage minimum charge C_{TSm}	0 kWh
Electrical storage charge limit P_{ESm}	0.75 kW
Electrical storage discharge limit P_{ESM}	0.85 kW
Thermal storage charge limit T_{ESm}	2.8 kW
Thermal storage discharge limit T_{ESM}	5 kW
Water heater converter efficiency η_{WH}	95%
PV array converter efficiency η_{PV}	10%
Electrical storage charge efficiency η_{ES}^{C}	86.5%
Electrical storage discharge efficiency η_{ES}^{D}	88%
Thermal storage charge efficiency η_{TS}^{C}	96.1%
Thermal storage discharge efficiency η_{TS}^{D}	96.1%
Electrical storage self-discharge rate D_{ES}	11 W
Thermal storage self-discharge rate D_{TS}	24 W
Forecast period T	24 hrs
Time step size Δt	1 min
Number of numerical time steps N_t	1440
Number of numerical charge steps N_c	100
Number of numerical control steps N_v	100

Table 1: Unit capacities, constraints, efficiencies, and optimisation parameters

4. Simulations

The optimal control model described in Section 3 was discretised with a semi-Lagrangian method in MATLAB using the flowchart in Fig. 3 as the basis of the code's structure. The code is made available as supplementary material to the paper, as a stand-alone library under the GNU GPLv3 license without dependencies on third-party solvers. The time needed to calculate the optimal control on a Windows 10 computer with an Intel i5-8250U (1.8 GHz) processor and 8GB RAM is 3.96 seconds per time step t. Moreover, the algorithm can be readily extended to include variable time-steps [35] and receding horizon control.

The optimal controls are determined through the partial derivatives of the optimisation surface of the value function. Indeed, the proposed numerical scheme is guaranteed to deliver the optimal strategy, cf. Theorem 1 in Subsection 2.1.

A model of the residential building described in Section 3.1 was built in Simulink, in order to accurately represent the practical system that is tested in Section 5. The simulated response was validated as having a 98.2% correlation with the hardware in the Moixa Test Laboratory, which is further described in Section 5. Moixa operates GridShare, a cloud-based aggregation server that connects storage devices to the grid to enable smart energy management. GridShare has a charging profile known as balance mode which can be applied to any connected storage de-

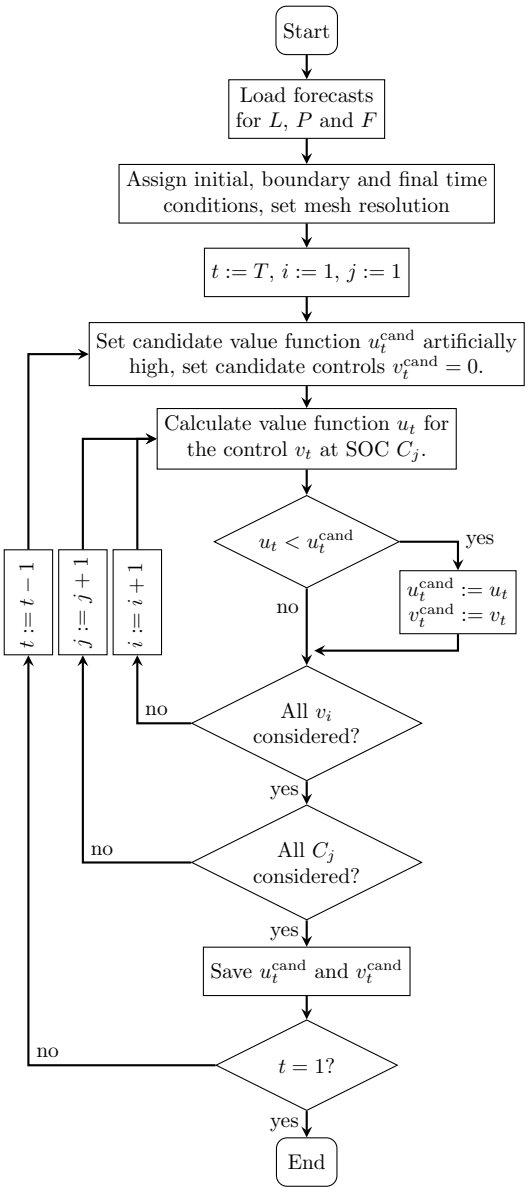

Figure 3: Optimisation model algorithm

vices. The basic logic is as follows, in order of priority:

1. Charge when there is excess PV energy.
2. Charge during periods of low cost energy.
3. Discharge when photovoltaic energy insufficient to satisfy load.
4. If the stored energy is insufficient for satisfying the load, the load is supplemented by the grid.

The balance mode profile is included in the Simulink model for comparison with the optimised results. As there are two energy storage devices in the model, it was assumed that balance mode would equally distribute any excess PV energy between the two devices; however, if one device is fully charged, the other device receives all the excess PV.

The winter and summer forecasts described in Section 3.1 were supplied to the MATLAB optimisation model, and the resulting optimal plans were downloaded to the Simulink test model. The Simulink model then used the same forecasts to evaluate the optimised response and the balance mode response. The electrical and thermal storage units were given a starting SOC of 2.4 kWh and 1.75 kWh, respectively.

	Base case daily cost	**Optimised daily cost**	**Saving**
Summer	£0.95	£0.74	29%
Winter	£2.14	£2.11	1.2%

Table 2: Cost and savings results from optimiser

4.1. Results & Discussion

The results in Table 2 show the optimiser is capable of providing a 29% saving to utility bills (in £/day) for the summer profile and 1.2% saving for winter.

The main benefits in these scenarios arise from the optimiser choosing between charging from low cost Economy 7 energy or waiting for excess PV energy, and controlling how the excess PV is divided between the storage units. The summer results are shown in Fig. 4 and demonstrate the above points. From 00:00 to 03:00 hours the optimised electrical storage device does not charge from low cost Economy 7 energy, this ensures capacity to absorb the excess PV energy from 09:00 to 15:00 hours instead of selling it to the Grid. When there is excess PV energy at 16:00 hours, the charging of the electrical storage device is observed to be prioritised; indeed, the thermal storage benefits from higher charging rates which allows it to exploit the short Economy 7 time slot more effectively.

In the caption of Fig. 4, 'electrical forecast' is the sum of the electrical load and PV generation forecasts. A negative value of electrical or thermal forecast denotes a load, whereas a positive value of electrical forecast is an excess. Positive battery response corresponds to charging, while negative is discharging. These results demonstrate a clear difference in strategies between the optimised and balance mode responses, which is particularly visible in the battery SOC profiles.

The optimised electrical storage response only partially charges during the low cost period to ensure sufficient capacity for charging from the excess PV energy. The optimised thermal storage response opts to not charge at all during the low cost period as there are no significant thermal loads until later in the day. The balance mode response however has both storage devices charging from low cost energy and saturated by 12:00 hours, with the unused excess PV sold to the grid.

The optimiser was stress tested using the summer dataset at a variation of starting SOC values for the storage units. These starting SOCs are shown along with the accompanying cost saving in Fig. 5. The results show a consistent cost saving for most combinations; however, there is a reduced saving available when both units start the day

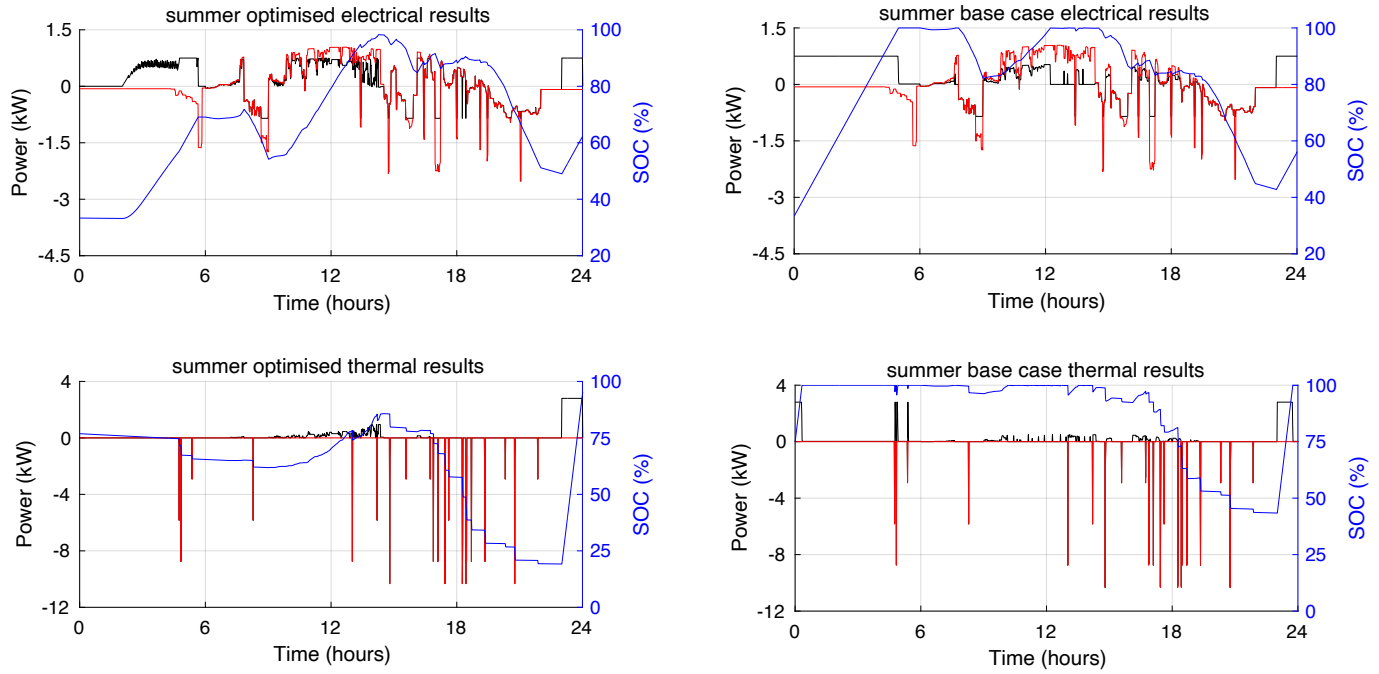

Figure 4: Summer electrical and thermal results with battery response (——), electrical/thermal forecast (——) and battery SOC (——)

.

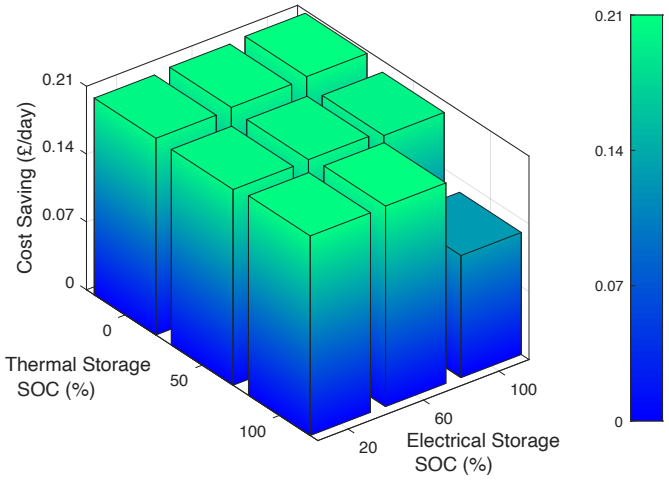

Figure 5: Summer cost saving vs. starting SOC

fully charged. This reduction is due to the particular profile of the loads. The excess PV energy is front loaded in the day but the optimiser has little chance to benefit from this as the storage units have no capacity to charge.

The controller may be supplied with imperfect forecasts. To test the effect of imperfect load forecasting, we provided it with a 24-hour forecasted load profile which deviates from the actually occurring load profile. The deviation involves a 1.6 kWh laundry cycle in the electrical load forecast which occurs at 18:00. The accurate forecast has full knowledge of this deviation, but the inaccurate forecast expects the laundry cycle to occur at 12:00. The results from this test showed that the inaccurate forecast was still capable of delivering 68.5% of the daily cost saving provided by the accurate forecast.

Because the entire statespace is mapped with the HJB method, the optimal control can still operate during forecast inaccuracies. The SOC will be different than predicted following a forecast inaccuracy, but the optimal control is calculated for all possible values of SOC at every time step. Therefore, sub-optimal control instructions will still exist and can be used until an updated forecast is available.

5. Experimental Validation

The optimisation model described in Section 3 was also implemented in C++ using the same basic structure as the MATLAB code in Section 4. The optimisation programme was then supplemented with extra code to manage the communication with the aggregation server and the energy storage devices. The algorithm structure is shown in Fig. 6. This code was installed on a Raspberry Pi microcontroller. It is capable of autonomously downloading forecasts from the aggregation server, optimising for a given period, and uploading optimal operating plans to the storage devices. This is in line with the "Coupled" practice as described by the IEEE 2660.1-2020 Recommended Practice [33]. Communication between the optimiser and the aggregation server is restricted to JavaScript Object Notation (JSON) format using Client URL (cURL) with secure authorisation tokens. This was managed in C++

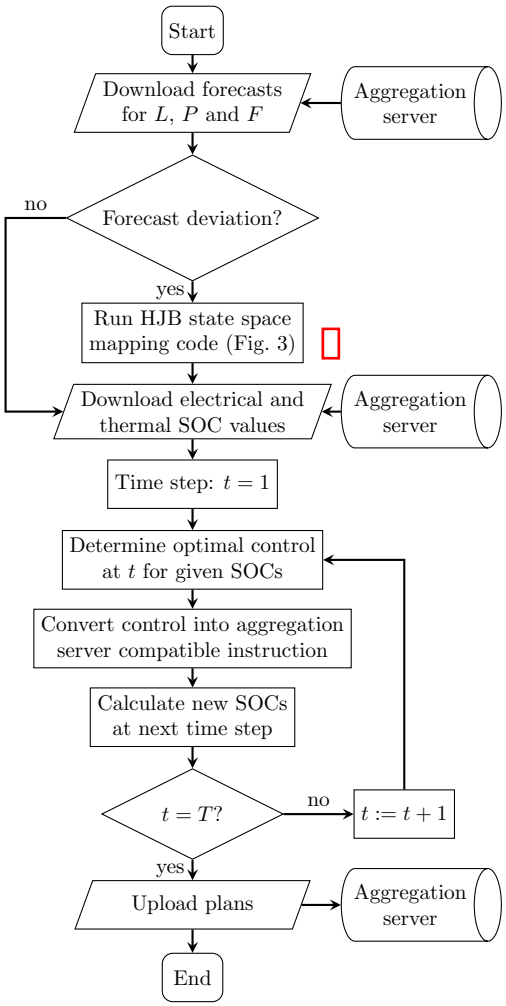

Figure 6: Raspberry Pi control algorithm

by implementing the jsmn [43] and cURL [44] libraries respectively.

The MATLAB Coder Toolbox was considered for generating the C++ code, however it was deemed unsuitable as it could not translate the mathematical functionality correctly. Instead the C++ code was, with minor exceptions, written from scratch. The code was initially tested on both a Bachmann MC205 Controller System and a Raspberry Pi computer. The Raspberry Pi was ultimately selected due to its open architecture and relative ease of wireless communication with the aggregator.

With this code, the time required to calculate the optimal approach on a Raspberry Pi 3 Model B+ is 1.6 seconds per time step or 38 minutes when T is 24 hours and discretisation parameter Δt is 1 minute. With a variable time step, which changes the step size after 4 hours to $\Delta t = 10$ minutes, the runtime is reduced to 10 minutes. This runtime is shorter than the MATLAB version of the model due to inherent efficiencies in the C++ language.

It is important to note that at this stage three distinct time scales are involved. Firstly, the above mentioned discretisation parameter Δt, which is chosen to balance

Function	**Duration (s)**	**Percentage of total**
Download forecasts	10	0%
Assign conditions	0.007	0%
Set mesh resolution	0.007	0%
Set u_t^{cand}	0.014	0%
Calculate u_t	2173.763	90%
Check if $u_t < u_t^{\text{cand}}$	35.638	1%
Update u_t^{cand}, v_t^{cand}	157.725	7%
Save u_t^{cand}, v_t^{cand}	0.107	0%
Download SOC values	10	0%
Determine optimal control	0.01	0%
Create server instructions	0.01	0%
Calculate new SOC values	0.5	0%
Upload plans	10	0%

Table 3: Unit capacities, constraints, efficiencies, and optimisation parameters

run-time with discretisation error (the latter being indicated qualitatively in Theorem 1). Secondly, the times at which the controller issues new controls to the storage units, which depends on the shape of the approximated value function as well as the instances at which the domestic residents interact with the power system. Generally these times are entirely independent of Δt. Thirdly, the frequency at which the HJB solution is updated, i.e. how often the optimisation part of the code is executed. This only happens when there is significant deviation between the new and the old forecasts. Because the entire state space is mapped with the HJB method, the optimizer does not need to be called as long as this deviation is sufficiently small (in contrast to a Pontryagin approach for instance which relies on exact forecasts). Thus, the run-time of the full optimisation code is not restricted by the time-step duration Δt or the incidence of user interactions, as is sometimes the case with other rolling optimisation methodologies.

In order to provide an understanding of the computational costs involved, the MATLAB Profiler tool was used to analyse the different parts of the code. The results can be seen in Table 3. It can be seen that the largest part of the computational time is taken by the above functionality.

The interactions between the Raspberry Pi, the aggregation server, the storage units, power sources, and loads are depicted in the energy hub diagram Fig. 7 and the experimental system diagram in Fig. 8. Each property in Fig. 7 can utilise different energy storage devices, power sources, and loads; the parameters would simply need to be altered on the individual Raspberry Pi.

The testing laboratory reflects a single property as these were shown in Fig. 7 and is comprised of the following commercially available hardware and testing equipment:

- Electrical storage: Moixa V4, 4.8 kWh,
- Thermal storage: Sunamp uniQ eHW3, 3.1 kWh,

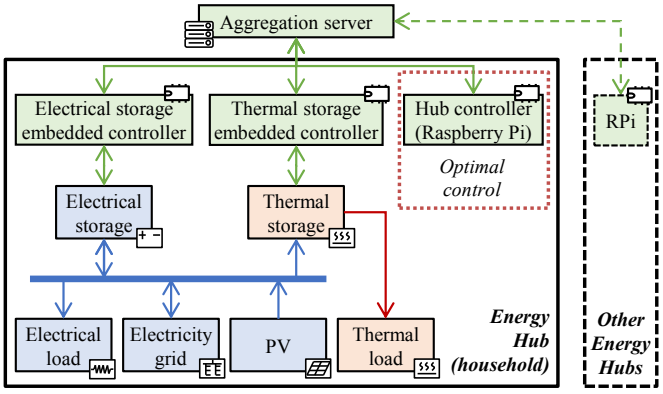

Figure 7: Energy Hub conceptual configuration with a hub controller. Lines indicate control signals (——), electricity (——) and heat (——).

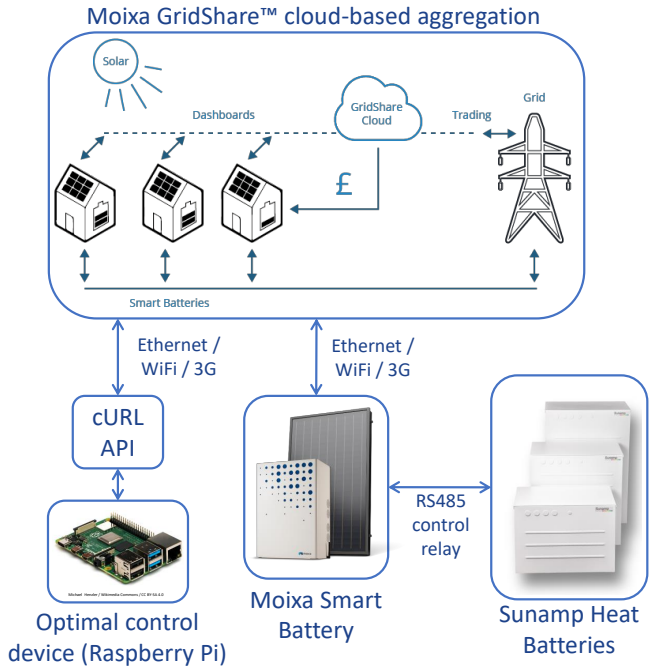

Figure 8: Experimental configuration of the system, including the controllers and electrical and thermal storage devices

- Electrical load: $15 \cdot 100$ W halogen lights,
- PV: 650 W solar PV simulator,
- Electrical grid: Local electrical supply,
- Thermal load: Hot water system with a 9 l/min flow rate,
- Communication: Wi-Fi link between the Raspberry Pi, the storage units, and the aggregation server.

A 25 minute test plan was created in the form of forecasts for the PV generation, electrical load, and thermal load. These forecasts were loaded onto the Raspberry Pi which followed the process described in Fig. 6 and uploaded optimal plans to the storage devices. The solar

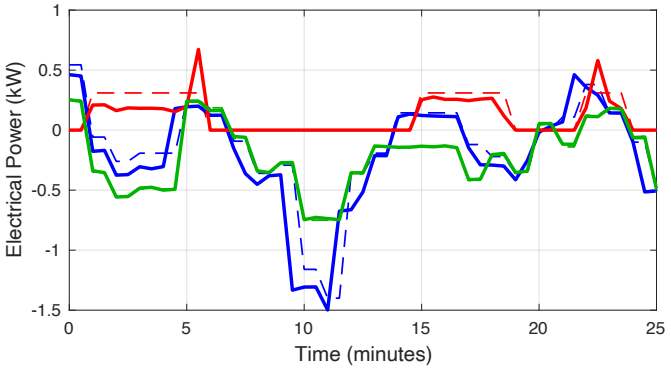

Figure 9: Experimental validation results with electrical load forecast (– – –), actual electrical load (——), electrical storage plan (– – –), electrical storage response (——), thermal storage plan (– – –) and thermal storage response (——).

PV simulator, electrical load, and thermal load were then all controlled manually with the aim of closely matching their forecasts. The net electrical load was 0.06 kWh, comprised of 0.24 kWh electrical load and 0.18 kWh solar PV generation. A total of 0.37 kWh of hot water was drawn as thermal load at varying intervals throughout the testing period. The thermal storage unit's electrical response trace as shown in Fig. 9 was reconstructed from the closed electrical circuit as the thermal charge data is not logged on the Sunamp device. It can be seen that the system was able to implement the plans successfully, with very small deviations. These deviations were mainly caused by the actual load variation against the forecast.

The purpose of this experimental procedure is to validate the complete system operation when every component is integrated and the system is fully functional with real domestic devices. The composition of the 25 minute test plan is chosen to include representative elements of a continuous operation within a domestic setting.

The experimental results demonstrate the functionality of the system in the following ways:

- The optimiser has been implemented in a prototype controller board, similar to the one that could be integrated in a storage product, and in accordance with IEEE 2660.1-2020 recommendations [33].
- The Raspberry Pi control board has been able to effectively connect to and communicate with the aggregator's system, in order to upload and download controls and measurements.
- The real electrical and thermal storage systems were shown to follow the controls sent to them by the experimental controller.
- Minor deviations between the forecasted and actual loads were implemented in a realistic way, which demonstrates the methodology's ability to flexibly respond to uncertainties.

6. Commercial value of the methodology

6.1. Wider benefits to society and the energy industry

The identified benefits of the proposed approach address all three elements of the energy trilemma, which is set between cost, emissions and security, as follows:

- **Reducing cost of energy**: The benefits of the proposed approach in electricity networks would materialise in the form of savings from necessary network upgrades to accommodate the new renewable and distributed energy resources (estimated annually at £63 / kWh installed). Apart from the network infrastructure, the proposed approach helps mitigate new generation needs that may arise, e.g. reserves for covering the variability of renewables, or peak plant capacity (estimated annually at £23 / kWh installed) [45].
- **Reducing emissions**: The method described in this paper demonstrates that storage can introduce the flexibility required by energy networks to reduce emissions. For example, solar energy can be stored during the day to be used in the evening, displacing gas or grid electricity use. Emissions can be reduced by:
  - facilitating increased renewable energy uptake and
  - emissions optimisation of joint electrical and thermal systems.
- **Improving security of supply**: Energy storage is key to improving security of supply. Aggregated storage is also useful for grid balancing, therefore avoiding black-outs or brown-outs. Supply security can be improved by:
  - providing a storage buffer for events such as temporary loss of generation capacity,
  - mitigating the variability of renewables to reduce network stress, as well as
  - by providing ancillary services.

6.2. Commercial value for the aggregator

The above methodology has been proven to work well with a commercial aggregator's software system. However, in order for it to be formally adopted, it needs to offer added value to the aggregator's business. The proposed methodology offers added value in the following ways:

- **Additional functionality**: The proposed approach enhances significantly the aggregator's capability of optimising the end user's device(s), ultimately saving them money. This is a powerful incentive for attracting more users, hence provides a competitive advantage to the aggregator.

	SOC headroom available daily	**Potential ancillary service fee income**
Electrical	0.62 kWh	£39.07
Thermal	0.80 kWh	£50.22

Table 4: Commercial benefit of proposed method for the aggregator

- **Resource heterogeneity**: The optimal control approach allows for the combined optimisation of multiple energy carriers, and a variety of different types of devices. This opens up a much wider market for energy resource aggregation, which has been predominantly based on electrical devices.
- **More headroom for ancillary service provision**: Optimising the use of devices across multiple energy carriers provides much greater flexibility for the aggregator to exploit, in order to provide services to distribution and transmission network operators, such as demand management and congestion relief.

The results in Table 4 demonstrate the additional income that the aggregator can incur by offering ancillary services with the extended headroom afforded by the proposed method. They also show the value of integrating heat into a storage aggregation and dispatch platform, showing that different energy vectors can be optimised in the home for customer benefits and dispatch for external services.

It was assumed that, as seen in Figure 4, the SOC of the optimised results was on average 13% lower for the electrical storage and 26% lower for the thermal storage. This allows for further exploitation of that SOC margin. It should be noted that the thermal storage margin can also be exploited for electrical ancillary services indirectly, through preventing electricity use for heating. An ancillary service provision fee of £63 / kWh was assumed [45]. The values shown are for a single day, and realistically ancillary service provision may happen scarcely, perhaps a few days per year.

Finally, in terms of the additional costs of implementing the proposed technique, these are minimal, and consist mostly of the new hardware requirement, as well as some additional maintenance costs. The prototype was implemented on a Raspberry Pi device, which costs less than £50, but contains several unnecessary features. An aggregator would be able to reduce those hardware costs with custom, cost-optimised hardware that remove these unnecessary features. If the control system is implemented robustly, it should not incur significantly more maintenance costs than existing low-level hardware in the aggregator's products.

7. Conclusions

This paper presents an experimentally validated framework for optimally controlling energy resource aggregators

with energy storage devices within a multiple energy carrier system. The Hamilton–Jacobi–Bellman framework incorporate nonlinear effects arising from storage degradation, conversion efficiency and self-discharge.

A semi-Lagrangian algorithm was developed and fully implemented in MATLAB and C++, which returns controls even when supplied inaccurate, single-valued forecasts. Moreover, we demonstrated that this HJB based approach is that it will approximate the globally optimal control strategy, see the Subsection 2.1.

The computational cost was found to be small, enabling on-line computations on a Raspberry Pi and which make the independent reliable operation in residential energy systems possible. The approach yields significant cost savings compared to conventional balance mode, up to £0.21 per day (Fig. 5) and 29% as in Table 2. This can offset any additional cost of the controller within a fraction of the system's lifetime.

The methodology of was work developed in agreement with the new IEEE 2660.1-2020 Recommended Practice, cf. [33].

Acknowledgement

This research was supported by the UK's innovation agency, Innovate UK, through Project Ref. 132934. The authors would like to thank their project partners Moixa Technology, Durham University, Sunamp & UK Power Networks Services. Max Jensen acknowledges the support of the Dr Perry James Browne Research Centre.

References

[1] M. Geidl, G. Andersson, A modeling and optimization approach for multiple energy carrier power flow, in: IEEE Russia PowerTech, 2005, p. MISSING (2005).

[2] P. Mancarella, MES (multi-energy systems): An overview of concepts and evaluation models, Energy 65 (2014) 1 – 17 (2014). doi:https://doi.org/10.1016/j.energy.2013.10.041.

[3] F. Kienzle, P. Ahčin, G. Andersson, Valuing investments in multi-energy conversion, storage, and demand-side management systems under uncertainty, IEEE Trans Sust Energy 2 (2) (2011) 194–202 (2011).

[4] H. Ibrahim, A. Ilinca, J. Perron, Energy storage systems—characteristics and comparisons, Renewable and Sustainable Energy Reviews 12 (5) (2008) 1221 – 1250 (2008). doi:https://doi.org/10.1016/j.rser.2007.01.023.

[5] M. H. Barmayoon, M. Fotuhi-Firuzabad, A. Rajabi-Ghahnavieh, M. Moeini-Aghtaie, Energy storage in renewable-based residential energy hubs, IET Generation, Transmission Distribution 10 (13) (2016) 3127–3134 (2016).

[6] R. Machlev, N. Zargari, N. Chowdhury, J. Belikov, Y. Levron, A review of optimal control methods for energy storage systems - energy trading, energy balancing and electric vehicles, Journal of Energy Storage 32 (2020) 101787 (2020).

[7] G. Bernasconi, S. Brofferio, L. Cristaldi, Cash flow prediction optimization using dynamic programming for a residential photovoltaic system with storage battery, Solar Energy 186 (2019) 233–246 (2019). doi:10.1016/j.solener.2019.04.039.

[8] Y. Yoon, Y.-H. Kim, Effective scheduling of residential energy storage systems under dynamic pricing, Renewable Energy 87 (2016) 936–945 (2016). doi:10.1016/j.renene.2015.09.072.

[9] G. Bao, C. Lu, Z. Yuan, Z. Lu, Battery energy storage system load shifting control based on real time load forecast and dynamic programming, in: IEEE International Conference on Automation Science and Engineering, 2012, pp. 815–820 (2012). doi:10.1109/CoASE.2012.6386377.

[10] F. Hafiz, A. De Queiroz, I. Husain, Coordinated control of PEV and PV-based storages in residential systems under generation and load uncertainties, IEEE Transactions on Industry Applications 55 (6) (2019) 5524–5532 (2019). doi:10.1109/TIA.2019.2929711.

[11] X. Feng, R. Glowinski, M. Neilan, Recent Developments in Numerical Methods for Fully Nonlinear Second Order Partial Differential Equations, SIAM Review 55 (2) (2013) 205–267 (2013). doi:10.1137/110825960.

[12] P.-L. Lions, Generalized solutions of Hamilton-Jacobi equations, Vol. 69 of Research Notes in Mathematics, Pitman (Advanced Publishing Program), Boston, Mass.-London, 1982 (1982).

[13] B. Heymann, J. Bonnans, P. Martinon, F. Silva, F. Lanas, G. Jiménez-Estévez, Continuous optimal control approaches to microgrid energy management, Energy Systems 9 (1) (2018) 59–77 (2018). doi:10.1007/s12667-016-0228-2.

[14] V. Amir, M. Azimian, Dynamic multi-carrier microgrid deployment under uncertainty, Applied Energy 260 (2020). doi:10.1016/j.apenergy.2019.114293.

[15] M. Roustai, M. Rayati, A. Sheikhi, A. Ranjbar, A scenario-based optimization of smart energy hub operation in a stochastic environment using conditional-value-at-risk, Sustainable Cities and Society 39 (2018) 309–316 (2018). doi:10.1016/j.scs.2018.01.045.

[16] M. Mohammadi, Y. Noorollahi, B. Mohammadi-ivatloo, M. Hosseinzadeh, H. Yousefi, S. T. Khorasani, Optimal management of energy hubs and smart energy hubs – a review, Renewable and Sustainable Energy Reviews 89 (2018) 33–50 (2018).

[17] M. A. Mirzaei, M. Nazari-Heris, K. Zare, B. Mohammadi-Ivatloo, M. Marzband, S. Asadi, A. Anvari-Moghaddam, Evaluating the impact of multi-carrier energy storage systems in optimal operation of integrated electricity, gas and district heating networks, Applied Thermal Engineering 176 (2020) 115413 (2020). doi:https://doi.org/10.1016/j.applthermaleng.2020.115413.

[18] F. Brahman, M. Honarmand, S. Jadid, Optimal electrical and thermal energy management of a residential energy hub, integrating demand response and energy storage system, Energy and Buildings 90 (2015) 65–75 (2015). doi:https://doi.org/10.1016/j.enbuild.2014.12.039.

[19] W. B. Powell, S. Meisel, Tutorial on Stochastic Optimization in Energy. Part II: An Energy Storage Illustration, IEEE Transactions on Power Systems 31 (2) (2016) 1468–1475 (2016).

[20] Moixa, Gridshare services, https://www.moixa.com/business-services/, accessed 10/03/2021.

[21] U. Das, K. Tey, M. Seyedmahmoudian, S. Mekhilef, M. Idris, W. Van Deventer, B. Horan, A. Stojcevski, Forecasting of photovoltaic power generation and model optimization: A review, Renewable and Sustainable Energy Reviews 81 (2018) 912–928 (2018). doi:10.1016/j.rser.2017.08.017.

[22] K. Amasyali, N. El-Gohary, A review of data-driven building energy consumption prediction studies, Renewable and Sustainable Energy Reviews 81 (2018) 1192–1205 (2018). doi:10.1016/j.rser.2017.04.095.

[23] S. Sen, V. Kumar, Microgrid control: A comprehensive survey, Annual Reviews in Control 45 (2018) 118–151 (2018). doi:10.1016/j.arcontrol.2018.04.012.

[24] T. Liu, D. Zhang, H. Dai, T. Wu, Intelligent modeling and optimization for smart energy hub, IEEE Transactions on Industrial Electronics 66 (12) (2019) 9898–9908 (2019).

[25] S. D. J. McArthur, E. M. Davidson, V. M. Catterson, A. L. Dimeas, N. D. Hatziargyriou, F. Ponci, T. Funabashi, Multi-agent systems for power engineering applications—part i: Concepts, approaches, and technical challenges, IEEE Transactions on Power Systems 22 (4) (2007) 1743–1752 (2007).

[26] S. Skarvelis-Kazakos, P. Papadopoulos, I. Grau Unda, T. Gorman, A. Belaidi, S. Zigan, Multiple energy carrier optimisation with intelligent agents, Applied Energy 167 (2016) 323 – 335 (2016). doi:https://doi.org/10.1016/j.apenergy.2015.10.130.

[27] H. Lin, Y. Liu, Q. Sun, R. Xiong, H. Li, R. Wennersten, The impact of electric vehicle penetration and charging patterns on the management of energy hub – a multi-agent system simulation, Applied Energy 230 (2018) 189 – 206 (2018). doi:https://doi.org/10.1016/j.apenergy.2018.08.083.

[28] M. C. Bozchalui, S. A. Hashmi, H. Hassen, C. A. Canizares, K. Bhattacharya, Optimal operation of residential energy hubs in smart grids, IEEE Transactions on Smart Grid 3 (4) (2012) 1755–1766 (2012). doi:10.1109/TSG.2012.2212032.

[29] M. Beus, F. Banis, H. Pandžić, N. K. Poulsen, Three-level hierarchical microgrid control—model development and laboratory implementation, Electric Power Systems Research 189 (2020) 106758 (2020). doi:https://doi.org/10.1016/j.epsr.2020.106758.

[30] E. Hossain, Z. Han, H. V. Poor, Smart grid communications and networking, Cambridge University Press, 2012 (2012).

[31] S. Bera, S. Misra, J. J. P. C. Rodrigues, Cloud computing applications for smart grid: A survey, IEEE Transactions on Parallel and Distributed Systems 26 (5) (2015) 1477–1494 (2015). doi:10.1109/TPDS.2014.2321378.

[32] F. Malandra, A. Kizilkale, F. Sirois, B. Sansò, M. Anjos, M. Bernier, M. Gendreau, R. Malhamé, Smart distributed energy storage controller (smartdesc), Energy 210 (2020) 118500 (2020). doi:https://doi.org/10.1016/j.energy.2020.118500.
URL https://www.sciencedirect.com/science/article/pii/S036054422031608X

[33] IEEE Recommended Practice for Industrial Agents: Integration of Software Agents and Low-Level Automation Functions, IEEE Std 2660.1-2020 (2021) 1–43 (2021). doi:10.1109/IEEESTD.2021.9340089.

[34] M. Bardi, I. Capuzzo-Dolcetta, Optimal control and viscosity solutions of Hamilton-Jacobi-Bellman equations, Systems & Control: Foundations & Applications, Birkhäuser Boston, Inc., 1997 (1997). doi:10.1007/978-0-8176-4755-1.

[35] M. Falcone, T. Giorgi, An approximation scheme for evolutive Hamilton-Jacobi equations, in: Stochastic analysis, control, optimization and applications, Birkhäuser Boston, Boston, MA, 1999, pp. 289–303 (1999).

[36] G. Barles, E. R. Jakobsen, Error bounds for monotone approximation schemes for parabolic Hamilton-Jacobi-Bellman equations, Mathematics of Computation 76 (260) (2007) 1861–1893 (2007). doi:10.1090/S0025-5718-07-02000-5.

[37] E. McKenna, M. Thomson, High-resolution stochastic integrated thermal–electrical domestic demand model, Applied Energy 165 (2016) 445 – 461 (2016). doi:https://doi.org/10.1016/j.apenergy.2015.12.089.

[38] Moixa, Smart battery, https://www.moixa.com/solar-battery/, accessed 10/03/2021.

[39] Sunamp, Sunamp heat batteries and thermal energy storage, https://www.sunamp.com/, accessed 10/03/2021.

[40] Npower, Npower energy tariff, https://www.npower.com/home/electricity-and-gas/products/fixed-long/, accessed 31/01/2018.

[41] Ofgem, Selling rate, https://www.ofgem.gov.uk/environmental-programmes/fit/fit-tariff-rates, accessed 10/03/2021.

[42] L. Grüne, J. Pannek, Nonlinear model predictive control, Communications and Control Engineering Series, Springer, 2017 (2017). doi:10.1007/978-3-319-46024-6.

[43] jsmn, JSON parser/tokenizer, https://github.com/zserge/jsmn, accessed 10/03/2021.

[44] cURL, Command line tool and library, https://curl.haxx.se/, accessed 10/03/2021.

[45] S. Daniel, S. Skarvelis-Kazakos, P. Jain, Local smart dc networks and distributed storage for reducing and shifting peak load, in: 22nd International Conference and Exhibition on Electricity Distribution (CIRED 2013), 2013, pp. 1–4 (2013). doi:10.1049/cp.2013.0934.